

## Antiproton-hydrogen annihilation at subkelvin temperatures

A. Yu. Voronin

*P. N. Lebedev Physical Institute, 53 Leninsky Prospect, 117924 Moscow, Russia*

J. Carbonell

*Institut des Sciences Nucléaires, 53, Avenue des Martyrs, 38026 Grenoble, France*

(Received 9 September 1996; revised manuscript received 27 October 1997)

The main properties of the interaction of ultralow-energy antiprotons ( $E \leq 10^{-6}$  a.u.) with atomic hydrogen are established. They include the elastic and inelastic cross sections and protonium (Pn) formation spectrum. The inverse Auger process ( $\text{Pn} + e \rightarrow \text{H} + \bar{p}$ ) is taken into account in the framework of a unitary coupled-channel model. The annihilation cross section is found to be several times smaller than the predictions made by the black sphere absorption models. A family of  $\bar{p}\text{H}$  near-threshold metastable states is predicted. The dependence of protonium formation probability on the position of such near-threshold  $S$ -matrix singularities is analyzed. An estimation for the  $\text{H}\bar{\text{H}}$  annihilation cross section is obtained. [S1050-2947(98)08505-9]

PACS number(s): 03.65.Nk, 34.10.+x, 11.80.Jy, 36.10.Dr

### I. INTRODUCTION

The unique features of the LEAR (low-energy antiproton ring) facility at CERN recently made possible the synthesis of a few antihydrogen atoms [1]. This effort was pursued by the antiproton decelerator (AD) project [2], and made possible the storage of sensible amounts of antihydrogen. This project reinforces the already active interest in investigating several theoretical and experimental problems in the physics of antimatter [3–7].

In view of storing antimatter in traps, it would be interesting to have some theoretical calculations of the rate at which antiprotons ( $\bar{p}$ ) and antihydrogen ( $\bar{\text{H}}$ ) annihilate with the residual gas. This process should be evaluated at subkelvin temperatures, the optimal energy domain for an effective synthesis and trapping of antimatter.

From a theoretical standpoint, a specific feature of systems like  $\text{H} + \bar{p}$  or  $\text{H} + \bar{\text{H}}$ , containing pairs of unlike charged heavy particles ( $p$  and  $\bar{p}$ ), is the possibility of rearrangement followed by protonium (Pn) formation. Indeed even at zero  $\bar{p}$  kinetic energy, protonium can be produced in states with principal quantum number  $n \leq 30$ .

Since the pioneer work of Fermi and Teller [8] in 1947, this problem has been treated by several authors [9–12] in the energy range going from a fraction to tens a.u. The usual approach is based on the following two assumptions: (i) the separation of electronic and nuclear motion, and (ii) the classical treatment of the antiproton dynamics. The aim of the present work is to provide a correct description of the ultralow-energy limit, i.e.,  $T_{\bar{p}} < 10^{-6}$  a.u., an energy domain in which the above-mentioned assumptions are no longer valid. As a consequence, we are definitely faced with a quantum three- or four-body problem.

In what follows we will consider the annihilation of ultraslow antiprotons with atomic hydrogen in the framework of a unitary coupled-channel approach. This process will be identified as the free Pn formation

$$\bar{p} + \text{H} \rightarrow \text{Pn}^* + e, \quad (1)$$

as far as the direct annihilation at such low energies can be neglected, and since further evolution of Pn states will result in annihilation.

In our treatment, the protonium formation as well as the virtual rearrangement process, i.e., the inverse reaction of Eq. (1),

$$\bar{p} + \text{H} \rightarrow \text{Pn}^* + e \rightarrow \bar{p} + \text{H}, \quad (2)$$

will be properly taken into account.

We will show that the energy dependence of the inelastic reaction probability is determined by a rich spectrum of near-threshold  $S$ -matrix singularities, corresponding to  $\text{H}\bar{p}$  near-threshold metastable states generated by the long-range charge-dipole interaction. Finally we will give an estimation of the  $\text{H}\bar{\text{H}}$  annihilation cross section in the energy range from  $10^{-8}$  to  $10^{-4}$  a.u.

### II. FORMALISM

An adequate formalism for the three-body problem can be found in the Faddeev equations [13], according to which three possible asymptotic clusters have to be explicitly described. In the case of slow antiprotons scattering on hydrogen, only two of them are physically important. The first one is the  $(pe)\bar{p}$  cluster, which corresponds to the elastic channel  $\text{H} + \bar{p} \rightarrow \text{H} + \bar{p}$ . The second one is the  $(p\bar{p})e$  cluster, corresponding to the protonium formation channels  $\text{H} + \bar{p} \rightarrow \text{Pn}^* + e$ .

A direct solution of the Faddeev equations for such a problem is made difficult by the large number of open channels containing fast oscillating asymptotics. In this section, we will develop a formalism which enables us to take into account the correct behavior of the three-body wave function in both above-mentioned asymptotic clusters, and benefit from the small value of the electron-antiproton mass ratio. We will show that this approach gives scattering observables with an accuracy of the order of  $\sim 10\%$  by using a very limited number of channels. At the same time, it provides a

transparent physical understanding of the low-energy three-body dynamics in the  $\bar{p}H$  reaction, which is the main aim of our study.

### A. Coordinate system

The Jacobi coordinates for the three-body problem are connected with the different possible asymptotic clusters. The coordinates corresponding to the elastic channel are defined by

$$\mathbf{r} = \mathbf{r}_e - \mathbf{R}_p, \quad \mathbf{R} = \mathbf{R}_p - \frac{m_e \mathbf{r}_e + M_p \mathbf{R}_p}{m_e + M_p}, \quad (3)$$

where  $\mathbf{r}_e$ ,  $\mathbf{R}_p$ , and  $\mathbf{R}_p^-$  are, respectively, the electron, proton, and antiproton coordinates, and  $m_e$  and  $M_p$  are the electron and proton mass.

It turns out that this frame is also convenient for describing the protonium production channels. Indeed, the  $p$ - $\bar{p}$  distance  $\rho = \mathbf{R}_p - \mathbf{R}_p^-$ , coincides within  $\mathbf{r}(m_e/M_p)$  with  $\mathbf{R}$  in Eq. (3). We will show that knowing the three-body wave function at  $\mathbf{r} \ll \rho(M_p/m_e)$  is enough to obtain a good approximation of the scattering observables. Thus we can substitute  $\rho$  with  $\mathbf{R}$ , and take into account, if necessary, the difference between  $\rho$  and  $\mathbf{R}$  in a perturbative way. Hereafter we will use the unique coordinate system (3).

### B. Three-body wave function

The three-body wave function is represented as a sum of two components, corresponding to the two considered clusters:

$$\Phi(\mathbf{r}, \mathbf{R}) = \Phi_1(\mathbf{r}, \mathbf{R}) + \Phi_2(\mathbf{r}, \mathbf{R}). \quad (4)$$

Component  $\Phi_1$  is supposed to describe the elastic channel, and can be written as

$$\Phi_1(\mathbf{r}, \mathbf{R}) = \sum_{\alpha} \phi_{\alpha}(\mathbf{r}) \chi_{\alpha}(\mathbf{R}), \quad (5)$$

where  $\alpha$  is the set of quantum numbers labeling the hydrogen atomic states  $\phi_{\alpha}$  as well as the corresponding antiproton wave function  $\chi_{\alpha}$ . From now on we will denote each term in the three-body wave function expansion like Eq. (5) as a ‘‘channel.’’

For an incident antiproton energy much smaller than the first hydrogen excitation threshold, it is convenient to select from Eq. (5) only the contributions which do not vanish in the asymptotics. This gives the simple form

$$\Phi_1(\mathbf{r}, \mathbf{R}) = \phi_{1s}(\mathbf{r}) \chi(\mathbf{R}). \quad (6)$$

It is useful to introduce a projection operator  $\hat{P}$ , which acts in the three-body state space and projects on the subspace of hydrogen states corresponding to open channels:

$$\hat{P} = \sum_{nlm} |\phi_{nlm}\rangle \langle \phi_{nlm}| \otimes \hat{1}. \quad (7)$$

In our case, the sum is limited to the  $1s$  state only. Component  $\Phi_1$  is then written

$$\Phi_1 = \hat{P} \Phi. \quad (8)$$

The second component  $\Phi_2$  describes all the remaining channels, and can be written in the form

$$\Phi_2 = (\hat{1} - \hat{P}) \Phi. \quad (9)$$

This means that all the electron states except  $1s$  contribute into  $\Phi_2$ , ensuring the orthogonality of both components. The  $\Phi_2$  component contains terms which correspond to the protonium formation channels. In order to take the asymptotic behavior of the cluster  $(p\bar{p})e$  into account explicitly,  $\Phi_2$  is expanded in a complete set of the  $(p\bar{p})$  eigenfunctions  $f_{\beta}(\mathbf{R})$ :

$$\Phi_2(\mathbf{r}, \mathbf{R}) = \sum_{\beta} g_{\beta}(\mathbf{r}) f_{\beta}(\mathbf{R}), \quad (10)$$

where  $g_{\beta}(\mathbf{r})$  are unknown expansion coefficients representing the electron wave functions in the channels characterized by protonium quantum numbers  $\beta$ .

Let us remark here that at this level no approximation has been made. In particular, the truncation done in choice (6) of  $\Phi_1$  is balanced in the functions  $g_{\beta}$  of the second component.

### C. Equations

The Schrödinger equation for a three-body vector state  $|\Phi\rangle$  reads

$$(\hat{H}_{ep} + \hat{H}_{pp}^{\text{ex}} + \hat{W}_{ep}^{\text{ex}} - E)|\Phi\rangle = 0, \quad (11)$$

with

$$\hat{H}_{ep} = -\frac{1}{2m_e} \Delta_r - \frac{1}{r} \quad (12)$$

the hydrogen Hamiltonian,

$$\hat{H}_{pp}^{\text{ex}} = -\frac{1}{2M} \Delta_R - \frac{1}{|\mathbf{R} + \mathbf{r}(m_e/M_p)|} \quad (13)$$

the protonium Hamiltonian, and

$$\hat{W}_{ep}^{\text{ex}} = \frac{1}{|\mathbf{R} - \mathbf{r}(1 - m_e/M_p)|} \quad (14)$$

the electron-antiproton interaction potential.  $M$  is the  $\bar{p}H$  reduced mass which, neglecting  $m_e/M_p$  terms, will be hereafter approximated by the protonium reduced mass  $M \approx M_p/2$ ;  $E = \varepsilon_B + E_{\bar{p}}$  is the total energy;  $\varepsilon_B$  is the hydrogen ground-state energy; and  $E_{\bar{p}}$  is the center of mass energy of incident antiproton. Note that all the spin degrees of freedom are neglected. We will first neglect the term  $\mathbf{r}(m_e/M_p)$ , and substitute the exact  $\hat{H}_{pp}^{\text{ex}}$  and  $\hat{W}_{ep}^{\text{ex}}$  by the approximations

$$\hat{H}_{pp}^{\text{ex}} = -\frac{1}{2M} \Delta_R - \frac{1}{R}, \quad \hat{W}_{ep}^{\text{ex}} = \frac{1}{|\mathbf{R} - \mathbf{r}|}.$$

Using Eqs. (8) and (9), we obtain the following coupled equations for the components  $|\Phi_i\rangle$ :

$$\begin{aligned}
& (\hat{H}_{p\bar{p}} + \hat{P}\hat{W}_{e\bar{p}}\hat{P} - E_{\bar{p}})|\Phi_1\rangle + \hat{P}\hat{W}_{e\bar{p}}(1 - \hat{P})|\Phi_2\rangle = 0, \\
& [\hat{H}_{e\bar{p}} + \hat{H}_{p\bar{p}} + (1 - \hat{P})\hat{W}_{e\bar{p}}(1 - \hat{P}) - E]|\Phi_2\rangle \\
& + (1 - \hat{P})\hat{W}_{e\bar{p}}\hat{P}|\Phi_1\rangle = 0. \tag{15}
\end{aligned}$$

Here we used the fact that  $\hat{P}$  commutes with  $\hat{H}_{e\bar{p}}$  and  $\hat{H}_{p\bar{p}}$ . The corresponding equations for the antiproton  $\chi(R)$  and electron wave functions  $g_\beta(r)$  could be obtained by substituting Eqs. (6) and (10) into Eq. (15). Due to the choice of the wave-function components, the solution of such a coupled-equation system will correctly describe the asymptotic behavior of the three-body system. This procedure will, however, remain formal, for it leads to an infinite set of coupled channels, including the closed ones, characterized by a continuous  $p\bar{p}$  momentum variable. To construct an equation system suitable for practical calculations, we should first analyze the contribution of different channels in expansion (10), in particular the one coming from the continuous spectrum. For such a purpose we represent  $\Phi_2$  as a sum of two components:

$$\Phi_2 = \Phi_2^d + \Phi_2^p, \tag{16}$$

where

$$\Phi_2^d(\mathbf{r}, \mathbf{R}) = \hat{F}\Phi_2(\mathbf{r}, \mathbf{R}) = \sum_{\beta}^{n_{\max}} g_\beta(\mathbf{r})f_\beta(\mathbf{R}), \tag{17}$$

$$\Phi_2^p(\mathbf{r}, \mathbf{R}) = (1 - \hat{F})\Phi_2(\mathbf{r}, \mathbf{R}) = \sum_{\beta=n_{\max}}^{\infty} g_\beta(\mathbf{r})f_\beta(\mathbf{R}), \tag{18}$$

and

$$\hat{F} = \sum_{\beta}^{n_{\max}} |f_\beta\rangle\langle f_\beta|. \tag{19}$$

$n_{\max}$  is a certain set of Coulomb quantum numbers chosen in such a way that  $\Phi_2^d$  contains all the open channels and, eventually, a limited number of closed ones. The sum from  $n_{\max}$  to infinity also includes the integration over the continuous  $\bar{p}$  momentum. The  $\Phi_2^d$  component describes the dynamics of protonium formation, and includes the corresponding asymptotics of the three-body wave function:

$$\lim_{r \rightarrow \infty} \Phi_2^d(\mathbf{r}, \mathbf{R}) = \sum_{\beta} f_\beta(\mathbf{R})S_\beta h_\beta^+(\mathbf{r}).$$

Here  $S_\beta$  are the  $S$ -matrix elements for the protonium formation, and  $h_\beta^+(r)$  are the outgoing electron waves in the channel with quantum numbers  $\beta$ . The component  $\Phi_2^p$  contains only closed channels.

At large  $R$  the component  $\Phi_2^d$  vanishes due to the Coulomb bound-state wave functions  $f_\beta$ . Conversely, the contribution from  $\Phi_2^p$  is essential as far as it contains nonvanishing terms coming from the  $p\bar{p}$  states in the continuum corresponding to the virtual excitations and breakup. It is shown in the Appendix that  $\Phi_2^p$  actually describes the effect of the

long-range polarization, which can be taken into account by introducing in the elastic channel the local potential

$$V_{\text{pol}}(R) = \frac{1}{2} \frac{\alpha(R)}{R^4}, \tag{20}$$

with  $\alpha(R)$  ensuring that for  $R \gg r_B$  (H Bohr radius)  $\alpha(R) \rightarrow -\alpha_d$  the H dipole polarizability. The following approximation [14] for  $\alpha(R)$  was found to be suitable in practical calculations:

$$\alpha(R) = \frac{2}{3} [R^5 + \alpha_d R^4 + 2\alpha_d R^3 + \frac{3}{2}\alpha_d(R^2 + R + \frac{1}{2})] e^{-2R} - \alpha_d.$$

It is qualitatively shown in the Appendix and proved by numerical calculations that at distances  $R \approx r_B$ ,  $\Phi_2^d$  dominates, and the main contribution to the wave function comes from the channels with  $n=26-40$ ; thus we can choose  $V_{\text{pol}}(R \ll r_B) \rightarrow 0$ .

We will first consider the case of total  $H\bar{p}$  angular momentum  $L$  equal to zero. The characteristic incident  $\bar{p}$  energy, below which the  $S$  wave dominates in the elastic channel, will be determined later.

It was shown in Ref. [15,16] that in the  $L=0$  case, protonium is primarily produced in states with angular momentum  $l=0$  and 1. The physical reason for this is that for the open channels with  $n=26-30$ , which dominate the reaction amplitude, the electron is ejected with rather small momentum  $k_e$ , and the centrifugal barrier reduces the probability to find a slow electron (and consequently protonium) with high angular momentum.

The preceding results enable us to construct a model which, including a limited number of channels, correctly describes the asymptotic behavior of the three-body wave function. These channels dominate the reaction amplitude, while closed channels corresponding to the continuous spectrum of protonium states are taken into account by means of the polarization potential (20). In practical calculations, we have included the protonium channels with principal quantum number  $n=10-40$  and angular momentum  $l=0$  and 1. Numerical checks showed the stability of the results when increasing the number of included channels. The considered equation system has the form

$$\begin{aligned}
& \left( -\frac{1}{2M} \partial_R^2 + \frac{L(L+1)}{2MR^2} + V_{\text{cs}}(R) + V_{\text{pol}}(R) - E + \varepsilon_B \right) \chi(R) \\
& + \sum_{n,l} \int \phi_{1s}(r) W_{0l}(r, R) f_{n,l}(R) \hat{\pi} g_{n,l}(r) dr = 0, \tag{21}
\end{aligned}$$

$$\begin{aligned}
& \sum_{n'l'} \left[ \left( -\frac{1}{2m} \partial_r^2 - \frac{1}{r} + \frac{l(l+1)}{2mr^2} + E_n \right) \delta_{nn',ll'} \right. \\
& \left. + \hat{\pi} U_{nn',ll'}(r) \hat{\pi} \right] g_{n',l'}(r) \\
& + \hat{\pi} \phi_{1s}(r) \int f_{n,l}(R) W_{l0}(R, r) \chi(R) dR = 0. \tag{22}
\end{aligned}$$

Here

$$V_{cs}(R) = -\left(1 + \frac{1}{R}\right)e^{-2R},$$

$$W_{0l}(r, R) = \frac{r_{<}^l}{r_{>}^{l+1}} \frac{1}{\sqrt{2l+1}},$$

$$U_{nn', ll'} = \int f_{n,l}(\mathbf{R}) f_{n',l'}(\mathbf{R}) \frac{1}{|\mathbf{R}-\mathbf{r}|} d^3\mathbf{R}, \quad \hat{\pi} = 1 - \hat{P} \delta_{0l},$$

and  $E_n = -E + (M/2n^2)$ .

#### D. Effective potential method

The numerical solution of Eqs. (21) and (22) is a rather difficult task, as far as each of the coupled integrodifferential equations includes fast oscillating functions  $\chi$  and  $f_n$ . A way to overcome this difficulty is by means of the effective potential method. This approach turned to be an efficient tool for both a qualitative understanding and a precise numerical treatment of the problem. The  $H\bar{p}$  scattering observables are given by the first equation for antiproton wavefunction  $\chi$  [Eq. (21)]. The effects of the remaining coupled equations (22) are taken into account by transforming the system (21)–(22) into one equation for  $\chi$  which contains a complex non-local effective potential

$$\left( -\frac{1}{2M} \partial_R^2 + \frac{L(L+1)}{2MR^2} + V_{cs}(R) + \hat{V}_{\text{eff}} + V_{\text{pol}}(R) - E + \varepsilon_B \right) \chi(R) = 0, \quad (23)$$

with

$$\hat{V}_{\text{eff}} = \sum_{nn', ll'} |f_{n,l}\rangle \langle \phi_{1s}| W_{0l}(r, R) \hat{\pi} \hat{K}_{nn'}^{ll'}(r, r') \times \hat{\pi} W_{l'0}(r', R') | \phi_{1s}\rangle \langle f_{n',l'}|. \quad (24)$$

Here  $\hat{K}_{nn'}^{ll'}(r, r')$  is the Green matrix of coupled equation system for electron wave functions:

$$\hat{K}_{nn'}^{ll'}(r, r') = \left\{ \left( -\frac{1}{2m} \partial_r^2 + \frac{l(l+1)}{2mr^2} + E_n - \frac{1}{r} \right) \delta_{nn'}^{ll'} + \hat{\pi} U_{nn'}^{ll'} \hat{\pi} \right\}^{-1}. \quad (25)$$

The whole problem is then split into two parts: to calculate the effective potential, and to solve the one-channel problem for antiproton scattering in a complex nonlocal potential.

The benefits of such an approach are varied. On the one hand, the Green function (25) is calculated by solving a coupled equation system for smooth electron wave functions, while the fast oscillating  $p\bar{p}$  wave functions are explicitly introduced by the well-known Coulomb states. On the other hand, the effective potential (24) practically does not depend on the  $\bar{p}$  incident energy in the domain  $E_{\bar{p}} \ll 0.01$  a.u. [15,16]. The minimum energy of the ejected electron (from a

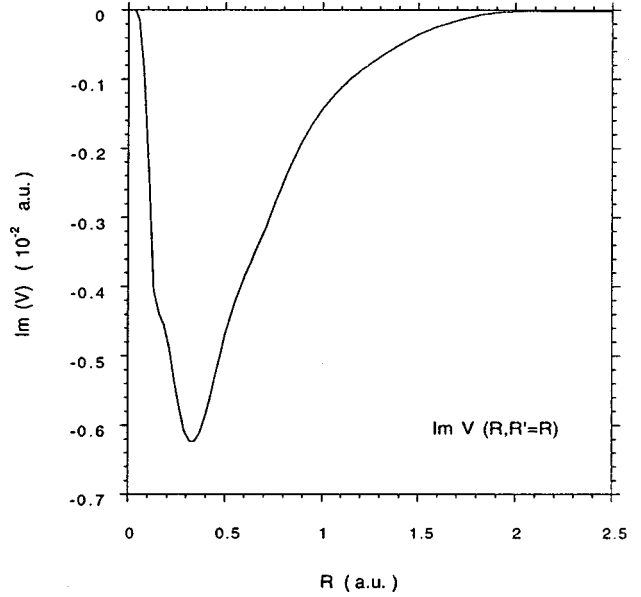


FIG. 1. Imaginary part of the effective potential  $V_{\text{eff}}(R, R' = R)$ .

$P_n$  state with  $n=30$ ) is about 0.02 a.u., and for  $\bar{p}$  energies less than this value, the Green matrix (25) is not sensitive to incident antiproton energy. This means that, once calculated for  $E_{\bar{p}}=0$ , the effective potential can be used in the whole energy range of interest, and this radically simplifies the calculations.

From a physical point of view, it also seems more natural to analyze the properties of the  $H\bar{p}$  system in terms of a modified one-channel problem. The main features of the effective potential as they appear from our calculations are the following.

(1) The imaginary part of  $V_{\text{eff}}$  vanishes at distance  $R \approx 1.8r_B$ , which corresponds to the mean radius of the last protonium open channel ( $n=30$ ). In Fig. 1,  $\text{Im}[V_{\text{eff}}](R, R')$  for  $R'=R$  is plotted as a function of  $R$ .

(2) The imaginary part of  $V_{\text{eff}}(R, R')$  is sharply peaked around its diagonal  $R'=R$ . Nevertheless, for  $R < r_B$ , the nonlocality range is of the same order as the antiproton wave function  $\chi(\mathbf{R})$  oscillation period. The profile of  $\text{Im}[V_{\text{eff}}](R, R')$  for  $R=0.5$  is shown in Fig. 2.

(3) The profile of the real part of  $V_{\text{eff}}$  is plotted in Fig. 3. Its nonlocality range is larger than for the imaginary part. It vanishes at  $R \approx 3r_B$ , and dominates over the polarization  $V_{\text{pol}}$  and the Coulomb screened  $V_{cs}$  potentials in the range  $1 < R < 3r_B$ .

### III. RESULTS

In this section, we will present the main results obtained in the coupled-channel model, and discuss the physical reasons of certain scattering observables behavior.

#### A. Scattering observables

The  $H\bar{p}$  complex scattering length is found to be

$$a = (-7.8 - i11.5)r_B.$$

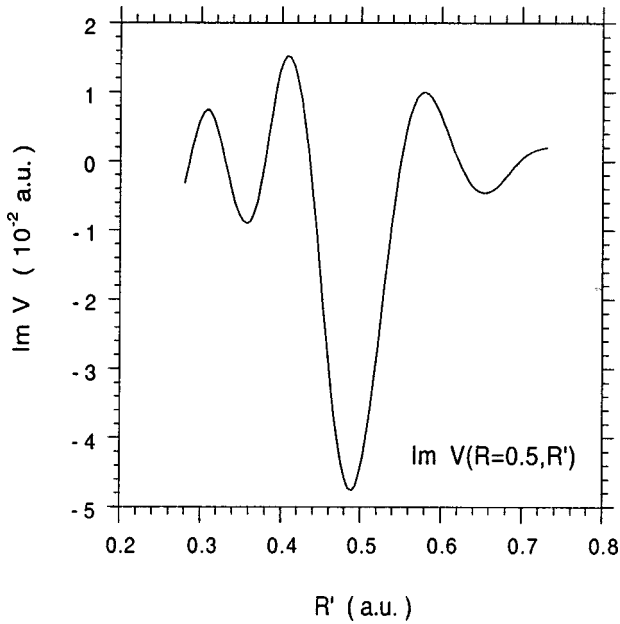


FIG. 2. Imaginary part of the effective potential  $V_{\text{eff}}(R=0.5, R')$ .

The corresponding elastic cross section at zero energy is

$$\sigma_{el} = 2426.4 r_B^2.$$

We remark on the relatively large value, on the atomic scale, of the scattering length imaginary part. Such a value is a consequence of the long-range polarization forces. By switching off  $V_{\text{pol}}$  in Eq. (23), the value obtained is substantially reduced to  $\text{Im}(a) = 0.2 r_B$ . The capital role of the polarization forces in the low-energy  $\text{H}\bar{p}$  dynamics will be discussed in Sec. III B.

We have calculated the energy dependence of the inelasticity  $S_r^2$  for several partial waves. The results are shown in Fig. 4 for  $\bar{p}$  incident energies in the range from 0 to  $10^{-6}$  a.u.

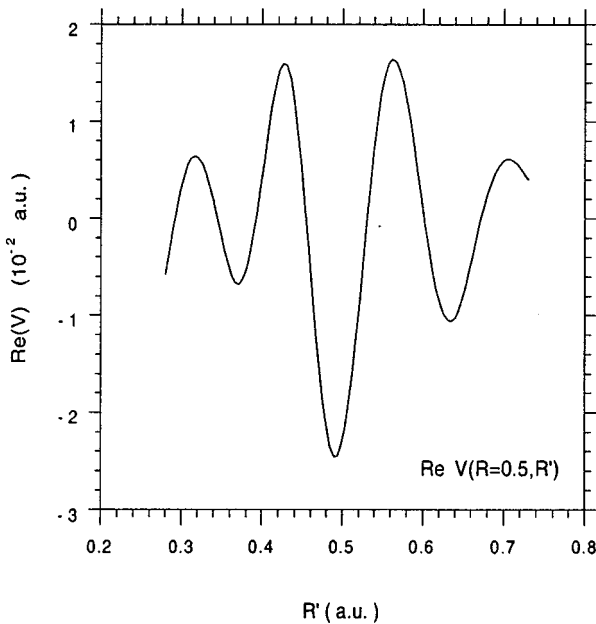


FIG. 3. Real part of the effective potential  $V_{\text{eff}}(R=0.5, R')$ .

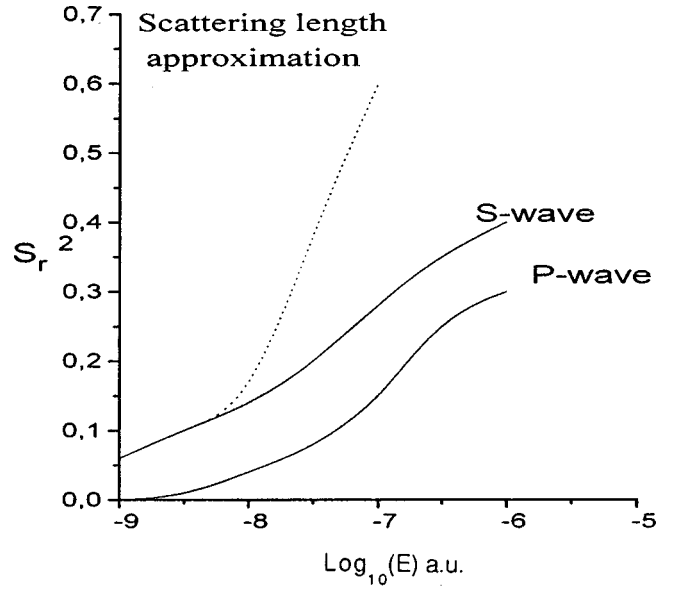


FIG. 4. Inelasticity  $S_r = 1 - |S|^2$  for the  $\text{H} + \bar{p} \rightarrow \text{Pn}^* + e$  reaction.

The inelasticity turns to be less than 0.1 for  $E_{\bar{p}} < 10^{-8}$  a.u., and does not become greater than 0.5 in the energy domain of interest. One can also see in this figure that the scattering length approximation is valid for energies less than  $10^{-8}$  a.u. The results for  $l \neq 0$  have been calculated under the assumption that the effective potential (24) depends weakly on total angular momentum  $L$  in the energy range of interest. As one can see, the  $S$  wave dominates for  $E_{\bar{p}} < 10^{-8}$  a.u.

The total annihilation cross section is shown in Fig. 5. It follows the  $1/v$  law for  $E_{\bar{p}} < 10^{-8}$  a.u., and decreases nonmonotonously for  $E_{\bar{p}} > 10^{-8}$  a.u. Such nonmonotonic behavior is originated by the contribution of nonzero angular momentum partial waves, which is explicitly seen in Fig. 4. It is interesting to compare this cross section with a semiclassical calculation [11] obtained under the following assumptions: (i) the  $\bar{p}$  motion can be treated classically, and (ii) the anni-

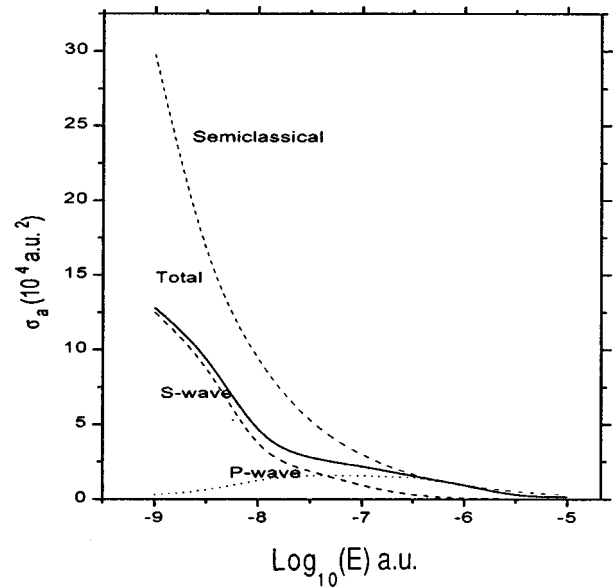


FIG. 5. Annihilation cross section for  $\text{H} + \bar{p} \rightarrow \text{Pn}^* + e$ .

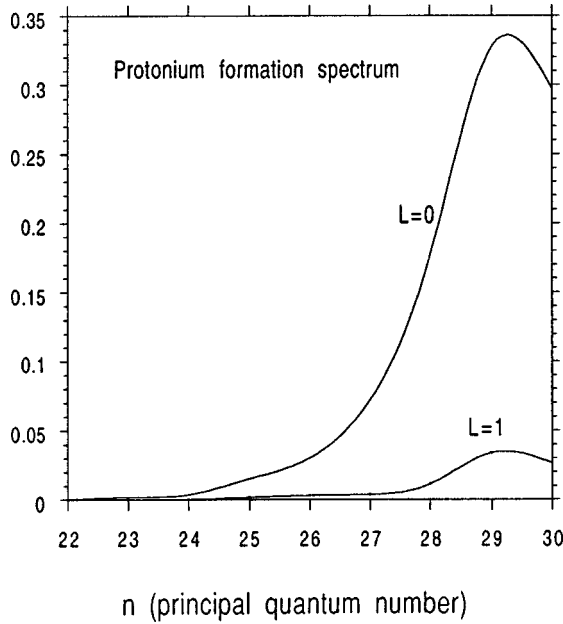


FIG. 6. Protonium formation probabilities in states with different quantum numbers.

hilation takes place with unit probability as soon as the  $\bar{p}$ -H distance is smaller than a critical radius  $R_c = 0.64r_B$ . The semiclassical cross section, shown in Fig. 5, is approximately 2.5 times larger than our values for  $E_{\bar{p}} < 10^{-8}$  a.u. This indicates that the low-energy  $\bar{p}$ H annihilation is sensitive to the quantum dynamics of protonium formation, and could hardly be reproduced with models in which the details of such dynamics are not taken into account.

The population of different protonium states, calculated for energies  $E_{\bar{p}} < 10^{-8}$  a.u. is shown in Fig. 6. Protonium is produced primary in the  $S$  states, with principal quantum number  $26 < n < 30$ . The  $P$ -states population does not exceed 15% of the whole captured fraction of antiprotons. These results confirm our qualitative estimation concerning the channels which make the main contribution to the reaction amplitude in the low-energy limit. It is worth to mention that the protonium  $S$ -states population dominates only for  $\bar{p}$  energies less than  $10^{-8}$  a.u., while the population of states with higher  $l$  should increase with increasing energy [17].

We conclude this paragraph by emphasizing that the  $H\bar{p}$  scattering observables significantly change their behavior at  $E_{\bar{p}} \sim 10^{-8}$  a.u., a characteristic energy for the reaction. We will demonstrate that this behavior is determined by the presence of near-threshold  $H\bar{p}$  bound and virtual states generated by the polarization potential.

### B. Near-threshold metastable states

The polarization potential is known to modify the low-energy cross sections of atomic reactions significantly. It plays an essential role in the  $H\bar{p}$  scattering. This potential produces a rich spectrum of  $H\bar{p}$  weakly bound and virtual states [18], which results from the long-range character of the polarization forces and the heavy (in atomic scale) antiproton mass. Such states, being near-threshold  $S$ -matrix sin-

TABLE I. Energies, Auger widths, and mean radii (a.u.) of  $L=0$   $H\bar{p}$  states. We denote by index I the results in  $V_{\text{pol}}$  alone, and by index II those obtained with the full interaction ( $V_{\text{pol}} + V_{\text{cs}} + V_{\text{eff}}$ ).

$E_I$	$E_{II}$	$\bar{x}_{II}$
	$-5.1 \times 10^{-8} + i7 \times 10^{-9}$	
$-4.2 \times 10^{-7}$	$-2.5 \times 10^{-6} - i0.2 \times 10^{-7}$	27.0
$-3.6 \times 10^{-5}$	$-7.0 \times 10^{-5} - i8.4 \times 10^{-6}$	11.3
$-2.6 \times 10^{-4}$	$-4.1 \times 10^{-4} - i3.2 \times 10^{-5}$	7.3
$-9.2 \times 10^{-4}$	$-1.5 \times 10^{-3} - i8.6 \times 10^{-5}$	5.3
$-2.3 \times 10^{-3}$	$-4.2 \times 10^{-3} - i2.0 \times 10^{-4}$	4.2

gularities, determine the energy dependence of the  $H\bar{p}$  scattering cross section. The main properties of such states and their relation with the observables are discussed in this subsection.

We first remark that the polarization potential  $V_{\text{pol}}$  alone generates several  $\bar{p}$  weakly bound states. The energy levels and mean radii of several nearest to the threshold  $S$  states produced by  $V_{\text{pol}}$  alone are shown in Table I (values marked by subscript II). These states are extremely prolonged, and have very small binding energies. By switching on the short-range part of the interaction, i.e., the complex nonlocal effective potential  $V_{\text{eff}}$  and the screened Coulomb  $V_{\text{cs}}$ , the spectrum is modified and inelastic widths appear. Nevertheless, the main features, small binding energy ( $10^{-8} < E_{\text{bound}} < 10^{-3}$  a.u.) and large radius ( $4 < \bar{x} < 27$ ) $r_B$ , remain.

In the threshold vicinity, the elastic  $S$  matrix for  $L=0$  is dominated by its singularities, and can be written in the form

$$|S|(k) = \prod_i \frac{|k + z_i|}{|k - z_i|}, \quad (26)$$

where  $z_i$  are the  $S$ -matrix poles with  $\text{Re}(z_i) < 0$  due to  $\text{Im}(V_{\text{eff}}) < 0$ . In Fig. 7 are shown the trajectories of several  $S$ -matrix poles ( $P_i$ ) and corresponding zeros ( $Z_i$ ) as a function of the strength of the  $V_{\text{eff}}$  imaginary part. As can be seen, the presence of the negative imaginary part in the effective potential results in shifting the  $S$ -matrix zeros to the right into the IV and I quadrants, with the corresponding symmetrical shift of  $S$ -matrix poles into the II and III quad-

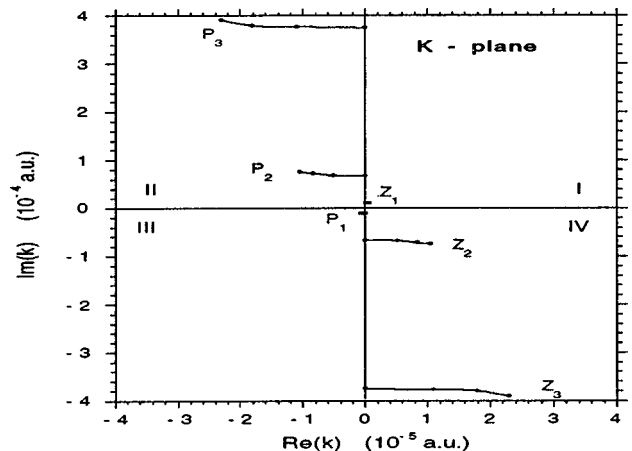


FIG. 7.  $S$  matrix near-threshold zeros ( $Z_i$ ) and poles ( $P_i$ ).

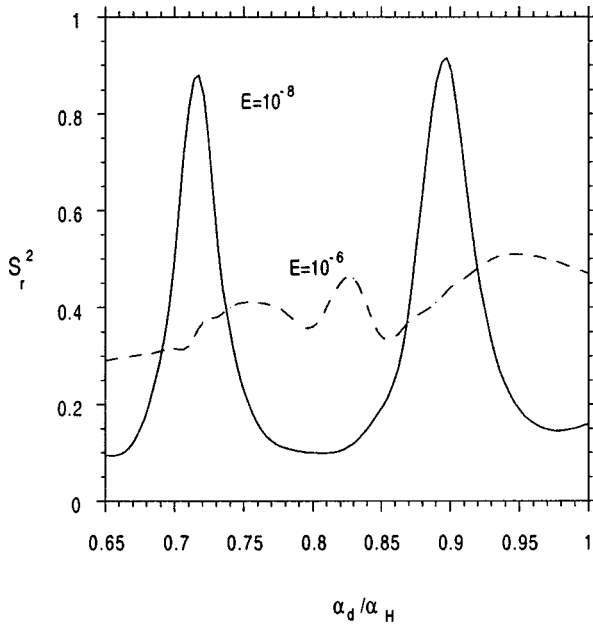


FIG. 8. Inelasticity for reaction  $H + \bar{p} \rightarrow \text{Pn}^* + e$  as a function of the dipole polarizability  $\alpha_d$ .

rants. The position of the  $S$ -matrix zero (and pole) nearest to the origin corresponds to an energy of  $E_c \sim 10^{-8}$  a.u., and plays the role of characteristic energy for reaction (1). We notice, however, that this  $S$ -matrix singularity nearest to the threshold lies on the nonphysical sheet, i.e.,  $\text{Re}(k) < 0$  and  $\text{Im}(k) < 0$ , and corresponds to a virtual state. Its wave function has an exponentially increasing asymptotic, and does not represent a physical state.

As the usual definition of effective range cannot be applied to the  $1/R^4$  polarization potential [14], we introduce the characteristic range of  $H\bar{p}$  interaction as  $R_A = 1/|k_0|$ , where  $k_0$  corresponds to the position of the  $S$ -matrix singularity nearest to the threshold. One can see that, for  $k \geq k_0$ , the scattering length approximation is no longer valid, and higher-order terms in the scattering amplitude expansion should be taken into account. With the result in Table I, one obtains  $R_A \sim 103$  a.u.

It is seen from Eq. (26) that for antiproton incident energies  $E_p \ll 10^{-8}$  a.u.,  $|k + z_i| \approx |k - z_i|$  and so  $|S| \rightarrow 1$ . This explains why the inelasticity  $S_r^2$  for  $E_p \ll 10^{-8}$  a.u. turns to be much less than unity. For  $E_p \gg 10^{-8}$  a.u., and because there are several  $S$ -matrix zeros situated to the right from  $-z_1$ , one has  $|k + z_i| < |k - z_i|$ , and the reaction probability increases.

To illustrate how the position of the near-threshold  $S$ -matrix singularities determines the low-energy scattering, we have calculated the inelasticity as a function of the dipole polarizability  $\alpha_d$  for a fixed energy ( $E_p = 10^{-8}$  and  $E = 10^{-6}$  a.u.) This function is plotted in Fig. 8. The strong oscillations between its maximum and minimum values with decreasing  $\alpha_d$  correspond to the motion of an  $S$ -matrix pole from the II to the III  $k$ -plane quadrant, while the symmetric  $S$ -matrix zero moves from the IV quadrant to the I quadrant. This means that a weakly bound state becomes virtual. As it is seen from Eq. (26), the inelasticity reaches its maximum value when an  $S$ -matrix zero crosses the real  $k$  axis.

This last result shows that sufficiently high accuracy of

calculations is required to obtain the scattering length value. At the same time, the reaction amplitude for energies  $E_p \gg 10^{-8}$  a.u. is less sensitive to the exact position of the near-threshold singularities, and can be more easily calculated. We estimate our accuracy in the scattering length results to be about 30%. This uncertainty appears mainly from the approximation used for  $V_{\text{pol}}$  at short distances. To obtain more precise results, one should increase the number of accounted closed channels, and take into account the difference between  $\rho$  and  $\mathbf{R}$  in Eq. (3). Such corrections seem not to be important for understanding the physics of the treated process, and are beyond the scope of the present paper.

We would like to emphasize that the near-threshold character of the above-mentioned  $S$ -matrix poles and zeros is determined by the long-range polarization potential. At the same time, their exact position in complex  $k$  plane cannot be obtained without a proper treatment of the protonium formation dynamics. In particular, the semiclassical black sphere condition does not hold in the energy domain  $E_p \leq 10^{-6}$  a.u. In terms of  $S$ -matrix analytical properties, the coupling with protonium production channels produces comparatively large (for the energy domain of interest) shifts of the real part of the  $S$ -matrix zeros, and reduces the inelasticity.

### C. Local approximation of the effective potential

It was shown that the energy dependence of the reaction probability is determined by the existence of several near-threshold states generated mainly by the long-range polarization forces. This suggests the possibility of obtaining a local complex potential which would be equivalent to the full  $H\bar{p}$  interaction in the energy range of interest. By ‘‘equivalent,’’ we mean not only to reproduce the same reaction probabilities but to support the same near-threshold spectral structure as well.

We search for such an equivalent local complex potential as a sum of three different terms

$$V_{\text{loc}}(R) = V_s(R) + V_{\text{cs}}(R) + V_{\text{pol}}(R),$$

$V_{\text{cs}}(R)$  and  $V_{\text{pol}}(R)$  being, respectively, the Coulomb screened and polarization potential used in Sec. III B, and  $V_s$  a local short-range part to be determined. It was assumed to have the form

$$V_s(R) = \begin{cases} -V_1 e^{-\alpha_1(R/r_B)} - iW_1 e^{-\beta_1(R/r_B)} & \text{if } R < R_c \\ -iW_2 e^{-\beta_2(R/r_B)} & \text{if } R \geq R_c, \end{cases} \quad (27)$$

and a satisfactory fit is obtained with the following parameter values:  $V_1 = 0.572$ ,  $W_1 = W_2 = 0.040$ ,  $\alpha_1 = 1.20$ ,  $\beta_1 = \beta_2 = 3.20$ , and  $R_c = 2r_B$ .

In Table II, the results of calculations in the nonlocal effective potential and abovementioned local approximation are compared. They agree within a few percent accuracy in the energy range  $0.5 \times 10^{-9} - 0.5 \times 10^{-6}$  a.u.

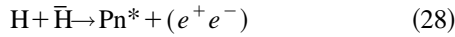
### D. Hydrogen-antihydrogen interaction

The results obtained for  $H\bar{p}$  interaction can be used for a qualitative treatment of different atom-antiproton ( $A\bar{p}$ ) and atom-antiatom ( $A\bar{A}$ ) system.

TABLE II. Inelasticity ( $S_r^2$ ) and  $S$ -matrix ( $S$ ) values calculated in the full effective potential (index I) and in its local approximation (index II) at different energies ( $E_{\bar{p}}$ ).

$E_{\bar{p}}$ (a.u.)	$S_r^2(\text{I})$	$S_r^2(\text{II})$	$S(\text{I})$	$S(\text{II})$
$0.5 \times 10^{-9}$	0.043	0.043	$0.978 + i0.01$	$0.978 + i0.014$
$0.5 \times 10^{-8}$	0.12	0.122	$0.937 + i0.013$	$0.936 + i0.021$
$0.5 \times 10^{-7}$	0.266	0.266	$0.836 - i0.185$	$0.836 - i0.177$
$0.5 \times 10^{-6}$	0.42	0.425	$0.023 - i0.756$	$0.034 - i0.757$

It is of particular interest to estimate the  $\text{H}\bar{\text{H}}$  annihilation cross section, and thus to examine the reaction:



The  $\text{H}\bar{\text{H}}$  system interacts at long distances via a dipole-dipole potential  $V_{\text{dd}} \sim -6.5/R^6$ . This potential also generates a spectrum of near-threshold states. Some of them, with  $L=0$ , are shown in Table III. In analogy with the case of Eq. (1), one can expect that the corresponding  $S$ -matrix singularities will determine the reaction dynamics of Eq. (28).

A qualitative estimation of the  $\text{H}\bar{\text{H}}$  potential can be obtained by adding to the same short-range part as in  $\text{H}\bar{p}$  case the dipole-dipole long-range tail  $V_{\text{dd}}$ . The reaction (28) cross section calculated in such a way is shown in Fig. 9. The characteristic energy for this reaction was found to be  $\sim 10^{-5}$  a.u., corresponding to the position of the  $S$ -matrix singularity nearest to the threshold (virtual state with energy  $-7.8 \times 10^{-6}$  a.u.).

A similar treatment can be used to estimate the inelasticity energy dependence for different  $A\bar{p}$  or  $A\bar{A}$  systems in the low-energy limit. For such a purpose, one has to find the  $S$ -matrix singularity nearest to the threshold, generated by polarization potential. The necessary condition for the validity of such a qualitative approach is that the characteristic range  $R_A$  of the  $A\bar{p}$  or  $A\bar{A}$  long-range interaction should be much greater than the inelastic range  $r_A$ .

As seen from Eq. (24), the inelastic range is mainly determined by the mean radius of the last protonium state open channel, and thus given by

$$\frac{M_A}{2n^2} = I_A, \quad r_A \approx \frac{2n^2}{M_A} = \frac{1}{I_A},$$

TABLE III. Energies, Auger widths, and mean radii (a.u.) of  $L=0\text{H}\bar{\text{H}}$  states. We denote by index I the results in  $V_{\text{pol}}$  alone, and by index II those obtained with the full interaction ( $V_{\text{pol}} + V_{\text{cs}} + V_{\text{eff}}$ ).

$E_{\text{I}}$	$E_{\text{II}}$	$\bar{x}_{\text{II}}$
$-7.8 \times 10^{-6}$	$-6.1 \times 10^{-6} + i1.8 \times 10^{-5}$	
$-1.9 \times 10^{-4}$	$-4.3 \times 10^{-4} - i2.2 \times 10^{-4}$	4.6
$-2.9 \times 10^{-3}$	$-5.2 \times 10^{-3} - i1.2 \times 10^{-3}$	2.8
$-1.1 \times 10^{-2}$	$-2.9 \times 10^{-2} - i8.4 \times 10^{-3}$	1.5
$-3.3 \times 10^{-2}$	$-5.8 \times 10^{-3} - i9.2 \times 10^{-3}$	1.3

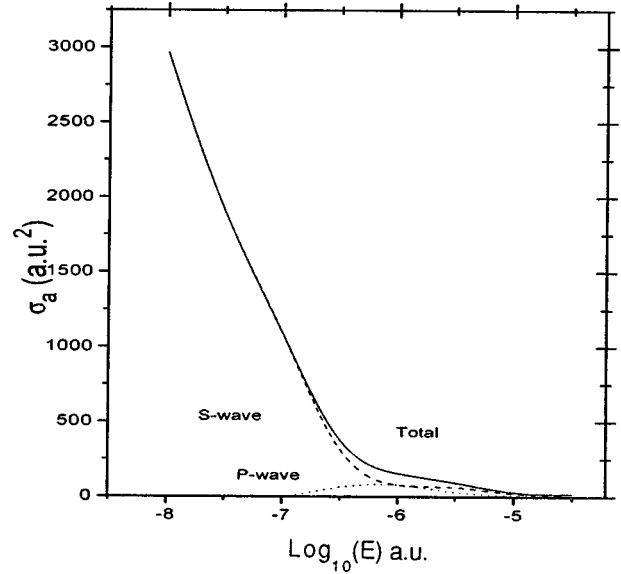


FIG. 9. Probability of reaction  $\text{H} + \bar{\text{H}} \rightarrow \text{Pn}^* + (e^+ e^-)$ .

where  $M_A$  and  $I_A$  are the  $A\bar{p}$  reduced mass and the first ionization potential, respectively, and  $n$  is the principal quantum number of the last open channel. A similar estimation for the  $A\bar{A}$  inelastic range  $r_{A\bar{A}}$  can be obtained if we take into account that Positronium is produced in this collision:

$$\frac{M_{A\bar{A}}}{2n^2} = 2I_A - \varepsilon_{\text{Ps}}$$

$$\varepsilon_{\text{Ps}} = I_{\text{H}}/2,$$

$$r_A \approx \frac{2n^2}{M_{A\bar{A}}} = \frac{1}{(2I_A - I_{\text{H}}/2)}.$$

Here  $M_{A\bar{A}}$  is the reduced mass of the  $A\bar{A}$  system,  $\varepsilon_{\text{Ps}}$  is the Positronium ground state energy.

As in the  $\text{H}\bar{p}$  case, the presence of near-threshold virtual states may considerably increase the characteristic range of  $A\bar{p}$  or  $A\bar{A}$  interaction. However, it can be interesting to have a simple approximation of this range in the aim of comparison with preliminary estimations (see also Ref. [12]). This is provided by the semiclassical condition for the number  $N$  of states:

$$\int \sqrt{2M_A V_{\text{pol}}^A} dR \approx \pi N.$$

This condition may be rewritten as follows:

$$\frac{R_A}{r_B} \approx \pi N.$$

For the  $A\bar{p}$  case, we obtain

$$R_A \sim \begin{cases} \sqrt{2M_A C_4^A} & \text{if } L=0 \\ \sqrt{2M_A C_4^A / L(L+1)} & \text{if } L>0, \end{cases} \quad (29)$$

while for  $A\bar{A}$  one has

$$R_A \sim \begin{cases} \sqrt[4]{2M_{A\bar{A}}C_6^A} & \text{if } L=0 \\ \sqrt[4]{2M_{A\bar{A}}C_6^A/L(L+1)} & \text{if } L>0, \end{cases} \quad (30)$$

$C_4^A$  and  $C_6^A$  being the atom charge-dipole and dipole-dipole van der Waals constants. Finally, we obtain the following ratio of inelastic and polarization range:

$$\frac{r_A}{R_A} = \begin{cases} \frac{1}{I_A \sqrt{2M_A C_4^A}} & \text{if } L=0 \\ \frac{\sqrt{L(L+1)}}{I_A \sqrt{2M_A C_4^A}} & \text{if } L>0 \end{cases} \quad (31)$$

for atom-antiproton, and

$$\frac{r_A}{R_A} = \begin{cases} \frac{1}{(2I_A - I_H/2) \sqrt[4]{2M_{A\bar{A}}C_6^A}} & \text{if } L=0 \\ \frac{\sqrt[4]{L(L+1)}}{(2I_A - I_H/2) \sqrt[4]{2M_{A\bar{A}}C_6^A}} & \text{if } L>0 \end{cases} \quad (32)$$

for atom-antiatom interaction.

Ratios (31) and (32), calculated for a wide range of different atoms, turn out to be much smaller than unity in the case  $L=0$ . In particular, for He, the less polarizable atom, they are  $\sim 0.02$  for  $\text{He}\bar{p}$ , and  $\sim 0.05$  for  $\text{He}\bar{\text{He}}$ . The polarization range dominates over the inelastic one in the partial waves up to  $L \sim 10$  for  $\text{He}\bar{p}$ , and  $L \sim 4$  for  $\text{He}\bar{\text{He}}$ . These values of  $L$  characterize the maximum angular momentum, which makes possible the existence of extended polarization states.

#### IV. CONCLUSION

A coupled-channel model describing the  $\text{H}\bar{p}$  system at energies less than  $10^{-6}$  a.u. has been developed. The results thus obtained substantially differ from the low-energy extrapolations of the black sphere model and other classical or semiclassical approaches. They show that such a low-energy requires a quantum-mechanical treatment in which the dynamics of the protonium formation is properly taken into account.

The effective  $\text{H}\bar{p}$  optical potential has been calculated in the framework of the coupled-channel model. In this framework, the  $\text{H}\bar{p}$  scattering length and zero-energy elastic cross section were found to be  $a = (-7.8 - i11.5)r_B$  and  $\sigma_{el} = 2426.4r_B^2$ , respectively. The  $\text{H}\bar{p}$  inelastic cross section has been calculated in the energy range from  $10^{-9}$  to  $10^{-6}$  a.u. It follows the  $1/v$  behavior up to energies  $\sim 10^{-8}$  a.u., where the scattering length approximation is valid. The inelasticity turned out to be much smaller than the black sphere model predictions.

The protonium formation spectrum for energies less than  $10^{-8}$  a.u. has been calculated. We have shown that the population of  $S$  states with a principal quantum number from 26 to 30 accounts for 75% of the total captured fraction.

The reaction dynamics is found to be determined by the existence of several near-threshold states. Such states are

produced by the long-range polarization potential, and are shifted in the complex momentum plane by the coupling with protonium formation channels. The  $\text{H}\bar{p}$  scattering length appears to be very sensitive to the position of the above-mentioned singularities, and requires accurate calculations.

A local approximation of the effective potential has been proposed for further applications. It reproduces the scattering observables in the considered energy range, and has the same near-threshold spectral properties. A qualitative extension of this approach to more general systems (atom- $\bar{p}$  and atom-antiatom) has been discussed.

The results discussed in this work have been obtained within an approximate model. In view of these, and motivated by the future project of storing antimatter at CERN, it would be interesting to check the validity of the different approximations by developing more accurate treatments including an exact solution of the three-body problem.

#### ACKNOWLEDGMENTS

The authors would like to thank I. S. Shapiro for suggesting the problem. One of the authors (A.V.) would like to thank D. Morgan for useful discussions.

#### APPENDIX A

The aim of this appendix is to find the dominant channels in expansion (10) of the three-body wave function. We first analyze the behavior of the component  $\Phi_2^p$  at distances  $R \gg r_B$ . The equation system for  $\Phi_2^d$  and  $\Phi_2^p$ , in terms of the projection operators  $\hat{P}$  [Eq. (7)] and  $\hat{F}$  [Eq. (19)] reads

$$\begin{aligned} & (\hat{H}_{p\bar{p}} + \hat{P}\hat{W}_{e\bar{p}}\hat{P} - E_{\bar{p}})|\Phi_1\rangle + \hat{P}\hat{W}_{e\bar{p}}(1 - \hat{P})\hat{F}|\Phi_2^d\rangle \\ & + \hat{P}\hat{W}_{e\bar{p}}(1 - \hat{P})(1 - \hat{F})|\Phi_2^p\rangle = 0, \end{aligned} \quad (A1)$$

$$\begin{aligned} & [\hat{H}_{ep} + \hat{H}_{p\bar{p}} + \hat{F}(1 - \hat{P})\hat{W}_{e\bar{p}}(1 - \hat{P})\hat{F} - E]|\Phi_2^d\rangle \\ & + \hat{F}(1 - \hat{P})\hat{W}_{e\bar{p}}(1 - \hat{P})(1 - \hat{F})|\Phi_2^p\rangle \\ & + (1 - \hat{P})\hat{F}\hat{W}_{e\bar{p}}\hat{P}|\Phi_1\rangle = 0, \end{aligned} \quad (A2)$$

$$\begin{aligned} & [\hat{H}_{ep} + \hat{H}_{p\bar{p}} + (1 - \hat{F})(1 - \hat{P})\hat{W}_{e\bar{p}}(1 - \hat{P})(1 - \hat{F}) - E]|\Phi_2^p\rangle \\ & + (1 - \hat{F})(1 - \hat{P})\hat{W}_{e\bar{p}}\hat{P}\hat{F}|\Phi_2^d\rangle \\ & + (1 - \hat{P})(1 - \hat{F})\hat{W}_{e\bar{p}}\hat{P}|\Phi_1\rangle = 0. \end{aligned} \quad (A3)$$

By taking into account that at large  $R$  the projection operator  $\hat{F}$  vanishes, Eqs. (A1)–(A3) simplify into the following system, valid for  $R \gg r_B$ :

$$(\hat{H}_{p\bar{p}} + \hat{P}\hat{W}_{e\bar{p}}\hat{P} - E_{\bar{p}})|\Phi_1\rangle + \hat{P}\hat{W}_{e\bar{p}}(1 - \hat{P})|\Phi_2^p\rangle = 0, \quad (A4)$$

$$\begin{aligned} & [\hat{H}_{p\bar{p}} + \hat{H}_{ep} + (1 - \hat{P})\hat{W}_{e\bar{p}}(1 - \hat{P}) - E]|\Phi_2^p\rangle \\ & + (1 - \hat{P})\hat{W}_{e\bar{p}}\hat{P}|\Phi_1\rangle = 0. \end{aligned} \quad (A5)$$

This system can be solved with respect to  $\Phi_2^p$ , and for the component  $\Phi_1$  gives

$$(\hat{H}_{pp} + \hat{P}\hat{W}_{ep} - \hat{P} - E_p)|\Phi_1\rangle + \hat{P}\hat{W}_{ep}(1 - \hat{P})\hat{G}_{\text{pol}} \times (1 - \hat{P})\hat{W}_{ep}\hat{P}|\Phi_1\rangle = 0, \quad (\text{A6})$$

in which

$$\hat{G}_{\text{pol}} = -[\hat{H}_{pp} + \hat{H}_{ep} + (1 - \hat{P})\hat{W}_{ep}(1 - \hat{P}) - E]^{-1}. \quad (\text{A7})$$

The last term in Eq. (A6) is the polarization long-range interaction

$$\hat{V}_{\text{pol}} = \langle \phi_{1s} | \hat{W}_{ep}(1 - \hat{P})\hat{G}_{\text{pol}}(1 - \hat{P})\hat{W}_{ep} | \phi_{1s} \rangle. \quad (\text{A8})$$

The asymptotics of the Green function  $\hat{G}_{\text{pol}}$  at  $R, R' \gg r_B$  is

$$G_{\text{pol}}(R, R', r, r') = \sum_{\alpha} \frac{1}{2p_{\alpha}} (e^{-p_{\alpha}|R-R'|} - S_{\alpha} e^{-p_{\alpha}(R+R')}) \phi_{\alpha}(r) \phi_{\alpha}(r'),$$

where  $p_{\alpha} = \sqrt{2M(|E - \varepsilon_{\alpha}|)}$ , and  $\alpha$  is a set of spherical Coulomb quantum numbers. If we take into account that at large  $R$ ,  $\hat{V}_{\text{pol}}$  acts on the very slowly changing function  $\chi(R)$  (the oscillation period of  $\chi$  for  $R \gg r_B$  is indeed much greater than  $r_B$ ), we can substitute  $G_{\text{pol}}$  in Eq. (A8) by the following expression:

$$G_{\text{pol}}(R, R', r, r') = \delta(R - R') \sum_{\alpha} \frac{\phi_{\alpha}(r) \phi_{\alpha}(r')}{E - \varepsilon_{\alpha}}.$$

By keeping terms up to  $1/R^4$ , we obtain the well-known charge-dipole potential asymptotic behavior

$$V_{\text{pol}}(R \gg r_B) = -\frac{\alpha_d}{2R^4},$$

$$\alpha_d = -2 \sum_{\alpha \neq (1s)} \langle \phi_{1s} | \hat{d} | \phi_{\alpha} \rangle \frac{1}{\varepsilon_B - \varepsilon_{\alpha}} \langle \phi_{\alpha} | \hat{d} | \phi_{1s} \rangle. \quad (\text{A9})$$

Here  $\hat{d}$  stands for the dipole momentum operator. In Eq. (A9) one recognizes the expression for the hydrogen dipole

polarizability,  $\alpha_d = \frac{9}{2}$ . We can thus conclude that the contribution of  $\Phi_2^p$  at large distances  $R$  can be taken into account by introducing, in the elastic channel, the polarization charge-dipole potential.

To estimate the contribution of different channels at distances  $R \approx r_B$  qualitatively, we first obtain the solution of Eq. (A1) in the distorted-wave approximation. Component  $\Phi_{1s}^0$ , obtained by neglecting the coupling to other components, is  $\Phi_1^0 = \phi_{1s}\chi^0$ , with  $\chi^0$  satisfying the equation

$$\left( -\frac{1}{2M} \partial_R^2 + V_{\text{cs}}(R) - E + \varepsilon_B \right) \chi^0 = 0.$$

The contributions of components  $\Phi_2^d$  and  $\Phi_2^p$  are characterized by the integrals

$$\langle \chi^0 \hat{P} | \hat{W}_{ep}(1 - \hat{P}) | \hat{F} \rangle, \quad \langle \chi^0 \hat{P} | \hat{W}_{ep}(1 - \hat{P}) | (1 - \hat{F}) \rangle. \quad (\text{A10})$$

An estimation of integrals (A10) can be obtained if we take into account the semiclassical character of the wave function  $\chi^0$  and the Coulomb wave functions at  $R \approx r_B$  in expansions (17) and (18). We are dealing with an integral of fast-oscillating functions which has significant values only if there exist stationary phase points inside the integration region. The equation for such stationary phase points is

$$\left( \frac{1}{R} + 1 \right) e^{-2R} = \frac{1}{R} - \frac{M}{2n^2}.$$

It can be shown that there are no stationary phase points for  $\Phi_2^p$ , while the contribution of  $\Phi_2^d$  at the distance  $R \approx r_B$  is mainly exhausted by protonium states with principal quantum number  $26 < n < 40$  (see Refs. [15,16]).

We have, in conclusion, that in the energy domain of interest and large internucleon distances the contribution of  $\Phi_2^p$  is the only important one, and can be taken into account by introducing the polarization potential (A8), while at the distances  $R \approx r_B$  the component  $\Phi_2^d$  dominates, and can be described by a limited number of channels. These qualitative arguments are important for a construction of the first approximation, and should be proved by further numerical calculations.

[1] G. Baur *et al.*, Phys. Lett. B **368**, 251 (1996).  
 [2] Fundamental studies of the antiproton at the AD, CERN/SPSLC 96-12/I207. In flight spectroscopy of antihydrogen at the proposed antiproton facility AD, SPSLC 96-25/M579.  
 [3] G. Gabrielse *et al.*, Hyperfine Interact. **81**, 5 (1993).  
 [4] G. Gabrielse *et al.*, Hyperfine Interact. **89**, 371 (1994).  
 [5] Proceedings of the Antihydrogen Workshop, edited by J. Eades [Hyperfine Interact. **76** (1993)].  
 [6] M. Charlton *et al.*, Phys. Rep. **241**, 65 (1994).  
 [7] *Proceedings of the Low Energy Antiproton Physics LEAP'94*,

edited by G. Kernel *et al.* (World Scientific, Singapore, 1995).  
 [8] E. Fermi and E. Teller, Phys. Rev. **72**, 399 (1947).  
 [9] D. L. Morgan, Jr. and V. W. Hughes, Phys. Rev. D **2**, 1389 (1970); W. Kolos, *et al.*, Phys. Rev. A **11**, 1792 (1975).  
 [10] B. R. Junker and J. N. Bardsley, Phys. Rev. Lett. **28**, 1227 (1972).  
 [11] D. L. Morgan, Jr., Hyperfine Interact. **44**, 399 (1988).  
 [12] G. V. Shlyapnikov *et al.*, Hyperfine Interact. **76**, 31 (1993).  
 [13] L. D. Faddeev, Tr. Mat. Inst. Akad. Nauk SSSR **1**, 69 (1963).  
 [14] N. F. Mott and H. S. W. Massey, *The Theory of Atomic Col-*

- lisions* (Clarendon, Oxford, 1965).
- [15] A. Yu. Voronin, Zh. Éksp. Teor. Fiz. **102**, 760 (1992) [Sov. Phys. JETP **75**, 416 (1992)].
- [16] A. Yu. Voronin and J. Carbonell, in *Proceedings of the International School of Physics of Exotic Atoms, Molecules and Their Interactions*, INFN/AE-94/24, edited by C. Rizzo and E. Zavattini (INFN, Trieste, 1994), p. 281.
- [17] E. Borie and M. Leon, Phys. Rev. A **21**, 1460 (1980); G. Reifenrother and E. Klempt, Nucl. Phys. A **503**, 885 (1989).
- [18] J. Carbonell, F. Ciesielski, C. Gignoux, and A. Voronin (unpublished); Few-Body Syst., Suppl. **8**, 428 (1995).